Adaptive Optics Imaging of Geographic Atrophy

Kiyoko Gocho,[1] Valérie Sarda,[1] Sabrina Falah,[1] José-Alain Sahel,[1] Florian Sennlaub,[2] Mustapha Benchaboune,[1] Martine Ullern,[1] and Michel Paques[1]

[1]Clinical Investigation Center 503, Centre Hospitalier National des Quinze-Vingts, Institute National de la Santé et de la Recherche Médicale (INSERM) and Université Pierre et Marie Curie-Paris6, Paris, France
[2]The Vision Institute, Centre de Recherche Inserm, Paris, France

Correspondence: Michel Paques, Clinical Investigation Center 503, INSERM and Centre Hospitalier National des Quinze-Vingts, 28 rue de Charenton, 75012 Paris, France; mp@cicoph.org.

Submitted: July 30, 2012
Accepted: February 27, 2013

Citation: Gocho K, Sarda V, Falah S, et al. Adapative optics imaging of geographic atrophy. *Invest Ophthalmol Vis Sci*. 2013;54:3673–3680. DOI:10.1167/iovs.12-10672

Purpose. To report the findings of en face adaptive optics (AO) near infrared (NIR) reflectance fundus flood imaging in eyes with geographic atrophy (GA).

Methods. Observational clinical study of AO NIR fundus imaging was performed in 12 eyes of nine patients with GA, and in seven controls using a flood illumination camera operating at 840 nm, in addition to routine clinical examination. To document short term and midterm changes, AO imaging sessions were repeated in four patients (mean interval between sessions 21 days; median follow up 6 months).

Results. As compared with scanning laser ophthalmoscope imaging, AO NIR imaging improved the resolution of the changes affecting the RPE. Multiple hyporeflective clumps were seen within and around GA areas. Time-lapse imaging revealed micrometric-scale details of the emergence and progression of areas of atrophy as well as the complex kinetics of some hyporeflective clumps. Such dynamic changes were observed within as well as outside atrophic areas.

Conclusions. In eyes affected by GA, AO NIR imaging allows high resolution documentation of the extent of RPE damage. This also revealed that a complex, dynamic process of redistribution of hyporeflective clumps throughout the posterior pole precedes and accompanies the emergence and progression of atrophy. Therefore, these clumps are probably also a biomarker of RPE damage. AO NIR imaging may, therefore, be of interest to detect the earliest stages, to document the retinal pathology and to monitor the progression of GA. (ClinicalTrials.gov number, NCT01546181.)

Keywords: geographic atrophy, adaptive optics, infrared imaging, retinal pigment epithelium

Geographic atrophy (GA), the atrophic form of AMD, is one of the most frequent causes of vision loss in industrialized countries.[1,2] In the past decade, notable progress in our comprehension of GA has been made, particularly the discovery of susceptibility genes that points to the involvement of chronic inflammation at the earliest stages of the disease.[3] However, despite these findings, the pathophysiology of GA remains poorly understood and there is currently no treatment for the disease.

Histologic studies[4–8] have shown that GA leads to a variable association of RPE and outer retinal degeneration, choriocapillary atrophy, infiltration by macrophages, and extensive redistribution of melanin-containing cells. More recently, knowledge about GA benefitted from progress in imaging technologies, which allowed a more convenient measure of the extent of lesions, of their progression, and of redistribution of ocular pigments. Adaptive optics (AO) fundus imaging is an optoelectronic technique allowing an order of magnitude improvement of the lateral resolution of retinal images as compared with conventional imaging.[9] To our knowledge, while AO imaging of the cone mosaic over drusens[10,11] or GA areas[12] has been reported, there has been no report of the use of AO imaging to document the pigmentary changes associated with GA at the microscopic level. Here, we performed flood illumination AO near infrared (NIR) imaging in patients affected by GA.

Methods

Patients

This single-center, institutional clinical study was carried out according to the principles outlined in the Declaration of Helsinki and was approved by the ethics committee of the Saint-Antoine hospital (Paris, France). Patients were recruited at the AMD clinic of the Quinze-Vingts Hospital. All participants gave their written, informed consent to participate. The cohort of patients comprised five women and four men with ages ranging from 62 to 91 years. All underwent a complete ophthalmologic examination including visual acuity measurement, optical coherence tomography (OCT), color fundus photographs, scanning laser ophthalmoscope (SLO) short wavelength (488 nm) and NIR (805 nm) autofluorescence (AF), and reflectance imaging (all with the Spectralis OCT-SLO; Heidelberg Engineering, Heidelberg, Germany). All presented features typical of mild to severe GA. All included subjects had refractions comprised between +2 and −3 diopters (D). Controls with ages ranging from 63 to 76 years and with a

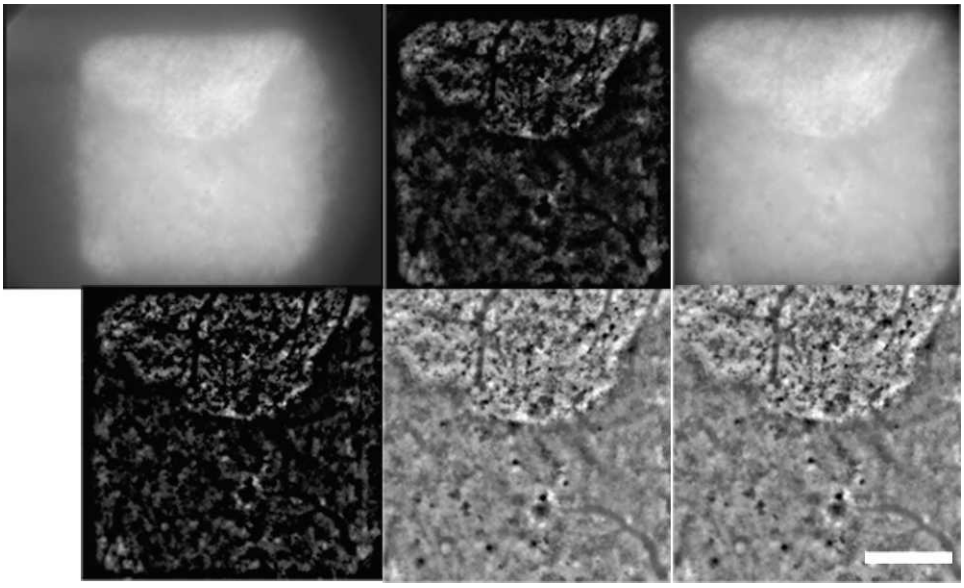

FIGURE 1. Step-by-step illustration of image processing (same image as in Supplementary Video S3). From *left to right* and *top to bottom*, the successive images obtained after the following steps: raw image, Sobel filtration, registration, subtraction of background, stretching of histogram, and oversampling (*scale bar*: 500 μm).

healthy ophthalmologic examination were also recruited during the same period.

Adaptive Optics Imaging Procedure

En face AO fundus images were obtained using an AO retinal camera (rtx1; Imagine Eyes, Orsay, France) that was previously decribed.[13] The rtx1 camera probes wavefront aberrations with a 750 nm super luminescent diode and a Shack-Hartmann detector (Haso 32-Eye; Imagine Eyes) and corrects them with a 52 actuators AO system operating in a closed loop. The fundus is illuminated with a temporally low coherent light emitting diode flashed flood source operating at 840 nm. The resolving power claimed by the rtx1 manufacturer (Imagine Eyes) is 250 line pairs per millimeter; this corresponds to a lateral resolution comprised between 2 and 4 μm. In the *z*-axis, the theoretical focus depth is 52 μm for a 5-mm pupil size and 35.7 μm for a 6-mm pupil.[14] Clinically, its depth of field is small enough to allow focusing on at least two levels in healthy retinas (Supplementary Fig. S1).

Pharmacologic pupil dilation using tropicamide (Mydriaticum, Novartis, France) was done in the seven cases where the pupil size was smaller than 4 mm. The imaging procedure is briefly summarized thereafter: the patient placed their head on a standard ophthalmic chin rest and was instructed to look at an internal fixation target, which is manually oriented by the operator to capture the region of interest (ROI). Focus was done at the cone photoreceptor layer by displacing a cursor in the software graphic user interface (rtx1 Software Suite; Imagine Eyes), while watching the live retinal image displayed by the monitor. Once the ROI has been detected and the focus adjusted, a stack of fundus images are acquired at a rate of 9.5 frames per second over 4.2 seconds in a $4^\circ \times 4^\circ$ area by a charged coupled device camera (Roper Scientific, Tucson, AZ). It is estimated that in emmetropic eyes each image covers a 1.2 $\times$ 1.2 mm area. An example of live fundus imaging is provided in Supplementary Video S1.

Image Processing

After each acquisition, the resulting series of 40 images was automatically processed by the system's software (rtx1 Software Suite; Imagine Eyes) as follows: The 20 images that presented the best contrast were automatically selected based on their average Sobel contrast. The Sobel contrast sum was computed by applying a classical Sobel filter to each image and averaging the absolute pixel values of the resulting filtered image. The 20 selected images were registered together using an algorithm based on auto-correlation, then added together in order to obtain a summed image with improved signal-to-noise ratio. A background image was computed by applying a Gaussian filter to the summed image. The SD of the Gaussian filter was 25 pixels. The background image was then subtracted from the summed image in order to facilitate the visualization of small details. The brightness and contrast of the resulting image were optimized by stretching the normalized histogram in order to cover the range from 0 to 1, while saturating the brightest pixels in the image. The number of saturated pixels was set to 0.05% of the total pixel number. Finally, the image was oversampled with a ratio of 1:2 using bicubic interpolation. Successive images obtained at each step are shown in Figure 1.

All these calculations were performed using double precision numbers and operators. The final images were stored in a 16-bit format. These images contain 1800 $\times$ 1800 pixels. It took approximately 30 seconds for the software (rtx1 Software Suite; Imagine Eyes) to apply the preceding algorithms and produce a final processed image. Each averaged image underwent visual control to ensure the absence of obvious rotational artifacts (i.e., blurry edges due to rotation of the eye during acquisition).

Composite images were constructed using i2k Align Retina software (DualAlign, LLC, Clifton Park, NY). For composite and multimodal imaging, rotation, size adjustment, and cropping were done as needed using Adobe Photoshop 7.0 (Adobe Corporation, Mountain View, CA).

Time-Lapse Imaging

In a subgroup of four patients, AO imaging was repeated with the primary purpose of documenting the progression of atrophy. The number of imaging sessions ranged from five to eight, with a mean interval between imaging sessions of 21

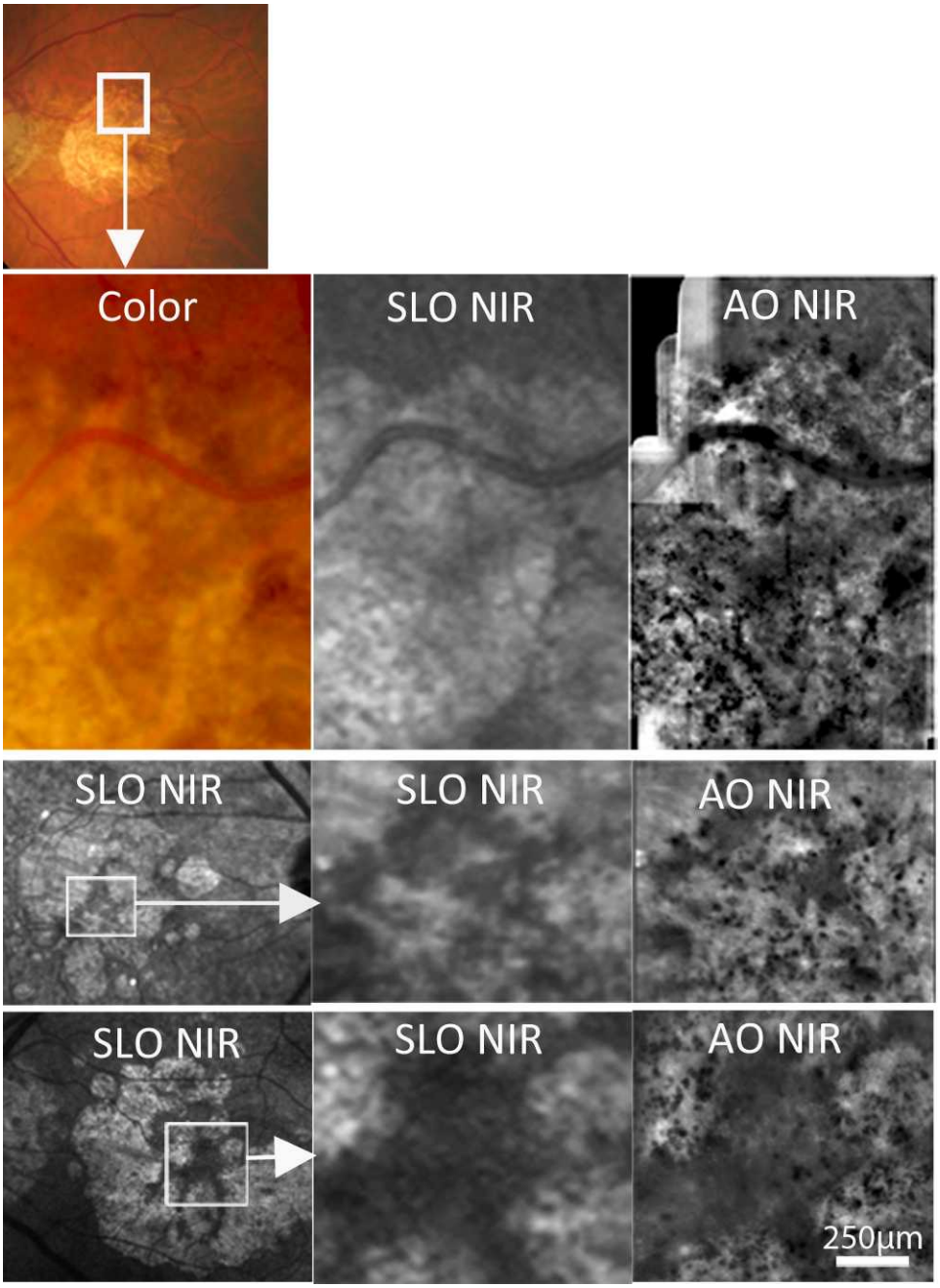

Figure 2. Comparison of color photographs, scanning laser ophthalmoscope (SLO), and AO-NIR imaging in three eyes with GA (from *top to bottom*: case 1, 2, and 3). Note by AO-NIR the better resolution of the borders and of the presence of hyporeflective clumps (HRCs) (*scale bar*: 250 µm).

days (range, 11–45) and a median follow up of 6 months (range, 3–7). The period between examinations was customized to the disponibility of each patient. To obtain time-lapse videos, averaged images of a given site were aligned and gif animations were constructed using i2k Align Retina software (DualAlign, LLC). To measure the progression of atrophy, the surface of individual GA spots on successive images were measured using ImageJ software (available in the public domain at rsb.inf.nih.gov/ij; National Institutes of Health, Bethesda, MD). The surface areas of GA lesions ($n = 5$) of cases six and eight were manually segmented using the loop tool. Each lesion was segmented independently by two operators (MP and SF).

Results

A comparison of NIR SLO and AO images in three representative cases is shown in Figure 2. This showed that, overall, AO imaging offered a better contrast of the limits of atrophic areas, and also showed the presence of a myriad of irregularly dispersed hyporeflective clumps (HRCs) up to 30 to 40 µm in diameter, within and around GA lesions. This gave a "salt and pepper" appearance to the posterior pole with a predominant "white" component. In some cases, high magnification of the largest clumps suggested that they were aggregates of smaller clumps (Fig. 3). In the case with the most clearly defined HRCs (Fig. 3, bottom), the average diameter (±SD) of the HRCs was 19.1 (±4) µm ($n = 12$). Measurement of HRCs in other eyes

Investigative Ophthalmology & Visual Science

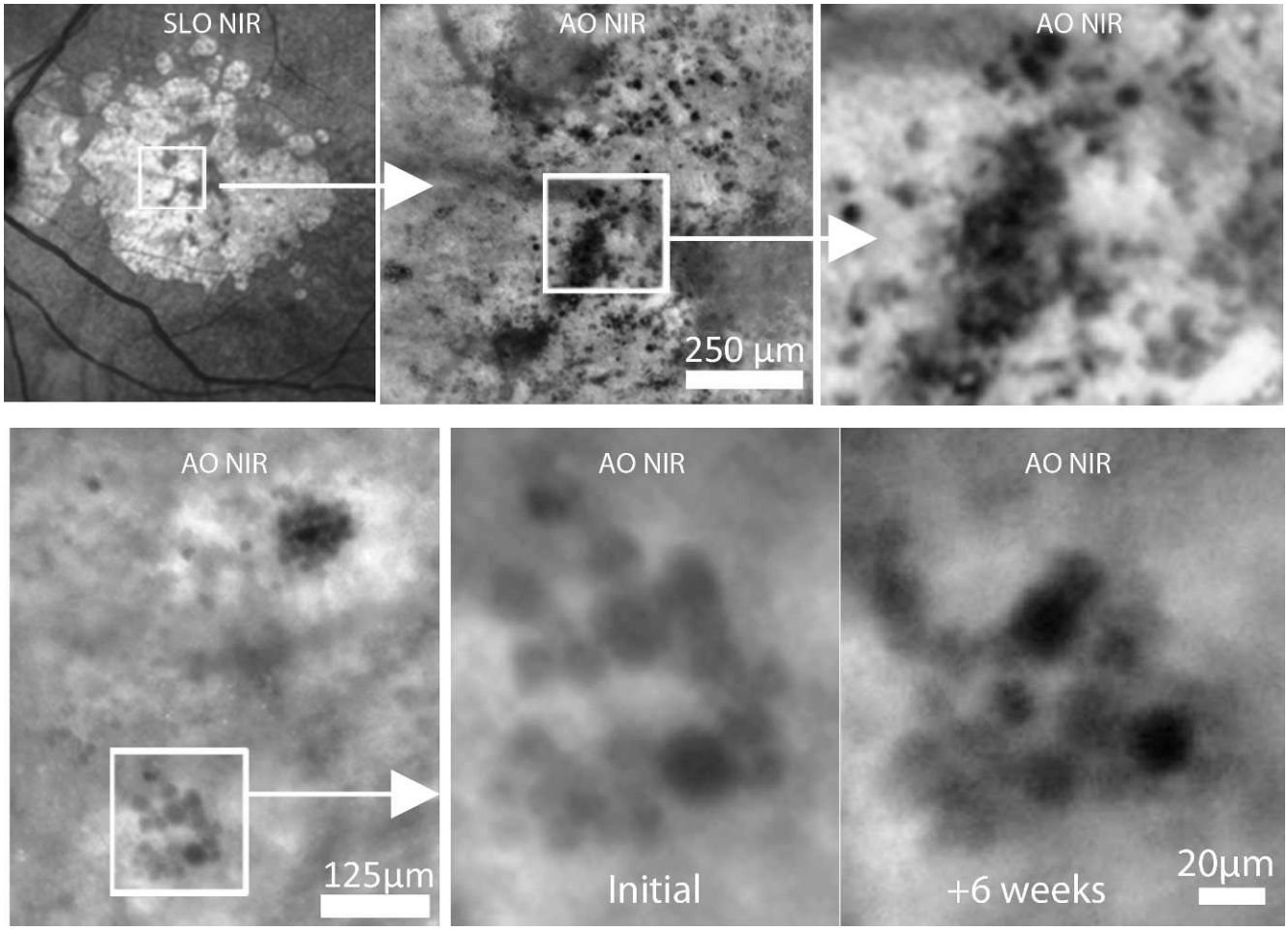

Figure 3. Comparison of large and small HRCs. AO NIR imaging of HRCs in two eyes with GA (*top row*, case 3; *bottom row*, case 4). In both cases high magnification AO imaging suggests that aggregates of small HRCs participate to the formation of large clumps. Note also in the *bottom row* the change in the distribution of these clumps over time.

could not be done with similar precision because of a less well defined border of the HRCs; nevertheless, their size distribution was in the same magnitude.

In the healthy-appearing retina adjacent to GA lesions, HRCs were also observed; although in a lower amount that in atrophic spots. The cone photoreceptor mosaic was also identified in the adjacent retina (Supplementary Fig. S2). In the macula of control subjects, features suggestive of HRCs could be suspected in many cases (Supplementary Fig. S3).

The pigment within these HRCs was investigated by comparing AO-NIR, NIR-AF (805 nm), and short-wavelength (488 nm) AF images (Fig. 4). Overall, although there was a certain degree of overlapping, large HRCs colocalized better with the distribution of NIR-AF than that of short wavelength-AF. For the smallest HRCs, however, the specific AF pattern was difficult to assess because of the intrinsic difference in resolution between SLO AF and AO imaging; thus, impairing pixel-to-pixel comparison.

In four patients we could investigate by time-lapse observations the kinetics of the progression of atrophy and of pigment redistribution. For this, successive AO images taken on an average of 3 weeks apart were registered. This allowed the observation of processes such as the emergence and/or progression of atrophic spots and the redistribution of HRCs (Figs. 5, 6, and Supplementary Videos S2–S7). Emergence of new GA spots was observed in two eyes of two patients. The progression of emerging GA areas is shown in Figure 4. GA areas doubled their area between 100 and 250 days after first detection. Interestingly, HRCs were detected at the earliest stage of their development, suggesting that HRCs appeared very early or even concomitantly to the onset of atrophy. Time-lapse observation also showed the dynamic aspect of the redistribution of HRCs (Figs. 3, 6, and Supplementary Videos S1–S7). The redistribution of HRCs over time varied among each lesion in a complex fashion. While limited changes were noted in some cases (Supplementary Video S5), many showed a more complex figure, with appearance of new clumps, change in their size and/or shape, rearrangement of large HRCs, or abrupt disappearance. Some HRCs were seen to migrate over small distances, in particular in the retina outside of atrophic lesions (Supplementary Videos S3, S4, S6).

Four eyes of four patients with foveal or parafoveal sparing were also examined (Fig 2, bottom row; Fig. 7; and Supplementary Videos S6, S7). Subfoveal HRCs were present in all cases. Time-lapse imaging performed in two of these cases showed that there was active redistribution of HRCs within and around the fovea (compare Supplementary Videos S6 and S7).

Discussion

Up to now, the main application of AO fundus imaging has been photoreceptor detection and counting; this somewhat

Investigative Ophthalmology & Visual Science

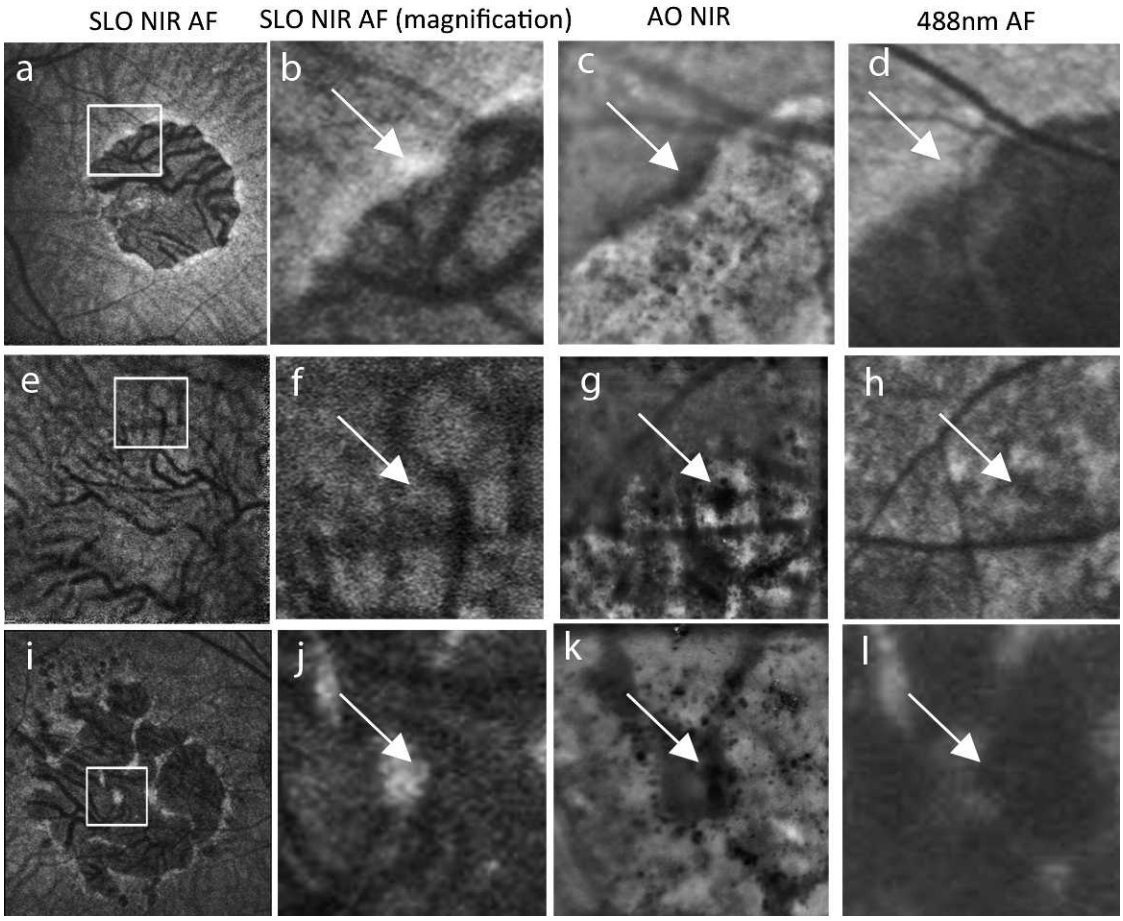

Figure 4. Comparison of NIR autofluorescence, short wavelength (488 nm) AF, and AO-NIR imaging in three eyes with GA (cases 5, 6, and 7). HRCs were rather congruent to the pattern of NIR-AF but to a lesser extent to that of short wavelength AF. *Arrows* points to HRCs showing increased focal NIR-AF without detectable focal increase of short wavelength-AF.

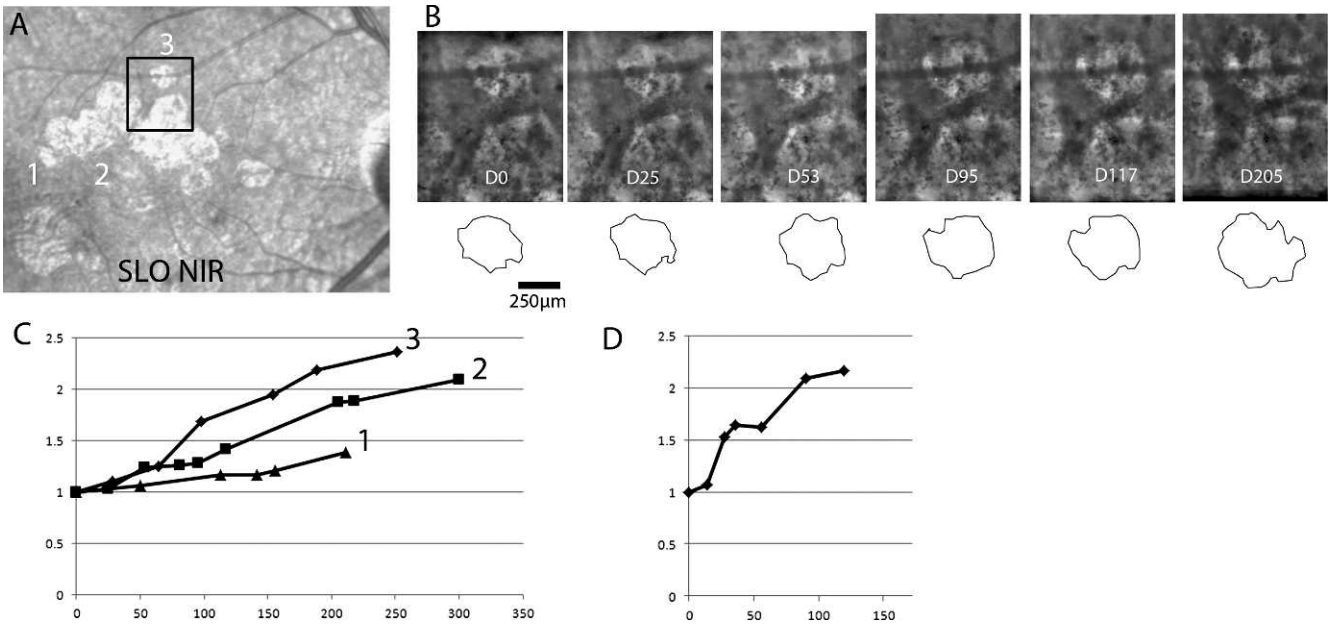

Figure 5. Illustration of the progression of small GA spots. *Top left*: SLO NIR imaging showing three GA spots (1, 2, and 3) in patient six. *Top right*: successive AO images of lesion 3, with the corresponding overlay. *Bottom row*: metrics of the progression of the surface of atrophy in GA spots (*x*-axis, duration from first detection of atrophy; *y*-axis, relative surface of the atrophic spot normalized to initial value) in patient six. Also shown is the graph of the progression of the small GA spot seen in Supplementary Video S4.

Investigative Ophthalmology & Visual Science

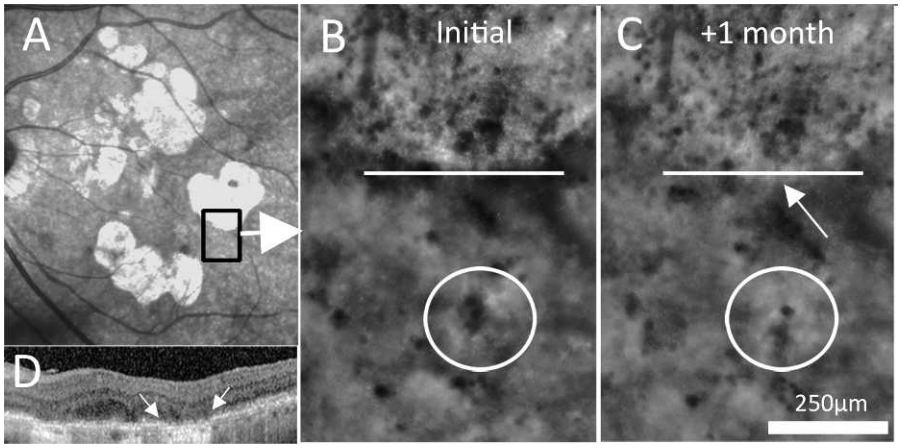

Figure 6. Illustration of progression of GA (Left eye of case 8). (**A**) SLO NIR image. (**B**, **C**) AO-NIR images taken 1 month apart. The *horizontal lines* and the *arrow* in (**C**) facilitate the identification of the progression of atrophy. Note also the rearrangement of HRCs outside of the atrophic area (compare the pattern of pigment distribution in the *circles*; see also Supplementary Video S3). *Arrowheads* points to a migrating clump. (**D**) OCT scan through the area of atrophy (*between arrows*).

shadowed the exploration of other retinal structures. In vivo imaging of the healthy RPE has been achieved experimentally[15] and also in patients with retinal dystrophy[16]; however, to our knowledge, there has been no report of high resolution imaging of pigment redistribution. Such investigation is of interest because redistribution of cellular material containing melanosomes, as AMD eyes contain both dysmorphic RPE and other cells containing melanosomes as part of presumed clearance activities (e.g., macrophages, Müller cells), is a biomarker of damage to the RPE. This occurs early in the process of AMD.[4,8] Patches of morphologically healthy-appearing RPE cells with reduced content of melanin may be observed on figures from histology reports of early phases of GA (such as in 17 of Ref. 4). At a subsequent step, there is heaping and sloughing of RPE cells, that may be followed by detachment and anterior migration of some RPE cells. At advanced stages of atrophy, melanin may be found in various locations: in ectopic RPE cells, in macrophages, or dispersed in the extracellular space in the form of melanosomes in pigment debris.

We show here that, although we could not identify the RPE mosaic, changes affecting the RPE may be as well accurately documented using AO imaging. This allowed detection of very small spots of atrophy and follow up of their progression, but also the detection of HRCs within as well as outside GA areas, which are likely to be as well indicators of RPE damage.

Accurate characterization of the progression of atrophic lesions during GA is important for the estimation of its long-term prognosis and consequently for the evaluation of therapeutic results. Using AO NIR imaging, we could measure the progression of emerging atrophic areas at a relatively small temporal and spatial scale. It is likely that improved imaging of small GA lesions may allow evaluating the effect of treatment at earlier stages of the disease, where such treatment may be more susceptible to show efficacy. Another interesting application of AO imaging would be the delimitation of the residual area of the retina in eyes with foveal sparing, which is challenging by conventional means.[17] High precision is indeed of utmost importance for these patients because a slight progression of atrophy may trigger catastrophic loss of central vision.

How the changes described by histology translate into in vivo imaging is a matter of speculation; yet, at the level of resolution currently achieved by AO, correlations between histology and AO NIR images can be discussed to some extent. We observed that large HRCs colocalized better with areas of increased NIR AF than short wavelength AF. Moreover, since melanin is the ocular pigment with the highest absorption and fluorescence rate in the NIR, it is possible that the HRCs

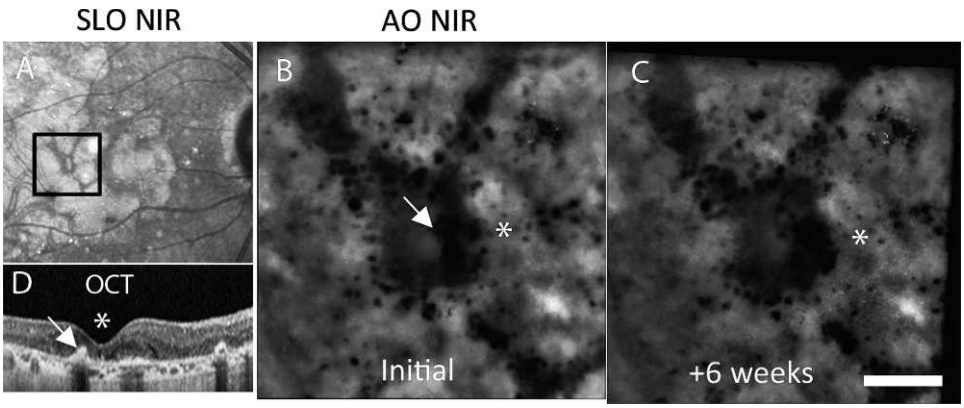

Figure 7. Multimodal imaging of the fovea (*asterisk*) of a case of GA with parafoveal sparing (case 7). (**A**) SLO NIR reflectance image. (**B**, **C**) Two AONIR images taken 6 weeks apart showing changes in the distribution of HRCs, in particular in the large parafoveal HRC (*arrow*; Supplementary Video S5). (**D**) OCT scan showing that the large HRC (*arrow*) is located at the level of the Bruch's membrane. *Scale bar*: 250 µm.

Investigative Ophthalmology & Visual Science

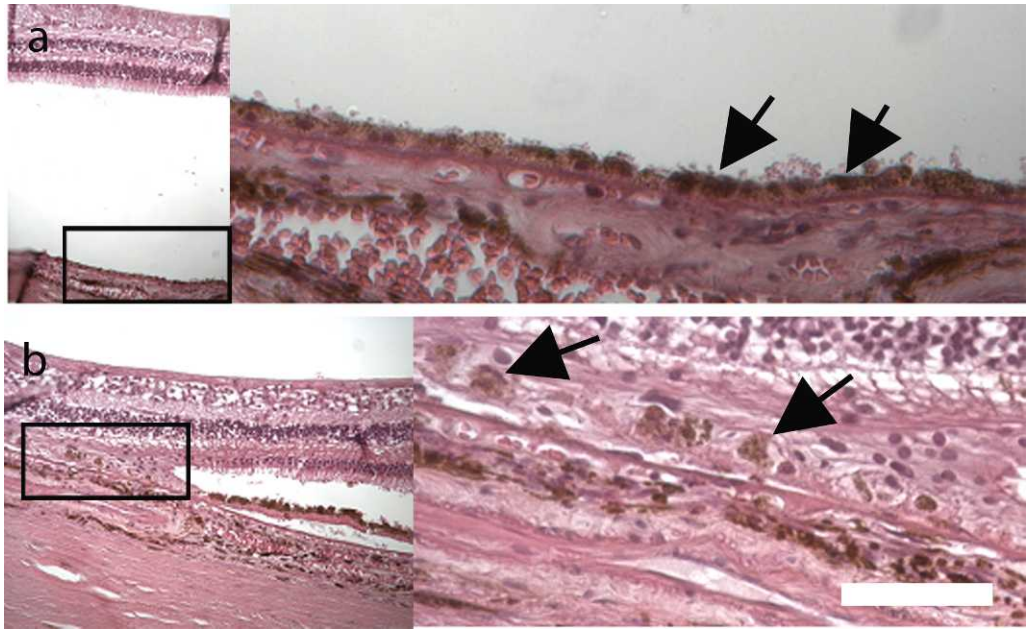

FIGURE 8. Histology of human cases of GA from donor eyes showing melanin dispersion outside (**a**) and inside (**b**) areas of geographic atrophy. *Arrows* points to melanin aggregates that may correspond to HRCs seen in vivo (Hematoxylin-eosin staining; *scale bar*: 50 μm).

observed by AO imaging are composed for some of them of melanin and/or its derivatives (such as melanolipofuschin). By histology, unevenness of melanin distribution is frequently observed within and outside GA areas (Fig. 8); these could therefore account for HRCs seen in vivo.

In vivo evaluation of RPE damage is commonly done by imaging the distribution of the two major pigments of the RPE, melanin and lipofuschin. Fundus short wavelength AF has been extensively used to map the distribution of lipofuschin,[18–21] a byproduct of the phagocytosis of photoreceptor outer segments. More recently, it has been shown that NIR reflectance and AF can detect melanin in vivo.[22–25] However, much less is known concerning in vivo imaging of melanin redistribution than of lipofuschin redistribution because of the more recent use and of the somewhat lower resolution of NIR imaging.

Although this could not be unequivocally demonstrated in all cases, especially for the smallest HRCs, our data suggest that AO imaging is of interest to document the redistribution of cellular material containing melanosomes; hence, changes affecting the RPE. Alternative explanation may account for HRCs such as the presence of other pigments (although hemoglobin is not known to be present in significant amount in GA cases) and also anisotropic dispersion of light. Outside of atrophic areas, small vessels parallel to the optical axis may absorb incident light enough to locally decrease reflectance. However, it is not the case in the fovea. Moreover, follow up studies showing motion of some of these clumps favors the hypothesis that they are melanin-containing cells. Some of the rounded HRCs observed in vivo in Figure 3 are indeed remarkably similar in size and shape to ectopic RPE cells reported by histology.[8] Heavily pigmented borders of atrophic area observed in patient eight may correspond to heaping and sloughing of the RPE described by histology. We also observed that HRCs undergo dynamic redistribution. Several nonmutually exclusive mechanisms may account for such kinetics. It is possible that detached RPE cells or macrophages slowly migrate in to the retina. Such random motility pattern is indeed reminiscent of that observed experimentally after a focal retinal insult, in which random-like motion of microglial cells was observed.[26] Hence, motion of melanin clumps may reflect the inflammatory background of GA such as the phagocytosis of dying RPE cells and/or the disruption of the RPE array. It is also known that, following RPE cell death, neighboring cells laterally expand to recover the Bruch's membrane. Hence, redistribution of HRCs may also be due to motion of melanosome aggregates within expanded RPE cells. One can also hypothesize that extracellular melanosomes circulate in the extracellular milieu within so called "debris."[8]

However, a large part of the observed redistribution did not fit into a migrating scheme; indeed, time-lapse observations showed that between two imaging sessions, some clumps changed their size, shape, and/or location, while others emerged and/or disappeared. It cannot be excluded that technical limitations such as defocusing or a mismatch between the sampling rate and the kinetics of migration account to some extent for the HRCs that could not be tracked. For instance, a pigmented cell moving anteriorly may become out of focus and, hence, disappear from the AO image; similarly, migrating melanin-containing cells cannot be reliably tracked if the delay between two imaging sessions is too long. Technical improvements of the AO technology and/or a closer follow up may overcome some of these difficulties.

In the fovea of subjects aged over 60 years, we frequently observed focal hyporeflectant spots roughly 20- to 50-μm diameter that are in some aspects similar to HRCs observed in patients. If they are indeed isolated RPE cells or melanin-loaded macrophages, they may indeed reveal a susceptibility to develop GA. Alternatively, it may indicate a "background" age-related redistribution of melanin. Additional studies are needed to clarify this.

In conclusion, we found that AO NIR imaging is of interest to detect the earliest occurrence of atrophic spots, to document the progression of GA at a small temporal and spatial scale, and also to investigate the dynamic process underlying the redistribution of HRCs, which are likely to be related to RPE damage. A complex, dynamic process of redistribution of HRCs indeed precedes and accompanies the emergence and progression of RPE atrophy. Further studies correlating AO NIR to conventional en face imaging and OCT

would help to better define the place of AO NIR imaging in the management of GA patients.

Acknowledgments

This work was presented in part at the ISIE/ARVO meeting, May 2012, Fort Lauderdale, Florida.

Supported by French Agence Nationale de la Recherche Grants ANR-07-LVIE-001 and ANR-09-TECS-009-01.

Disclosure: **K. Gocho**, None; **V. Sarda**, None; **S. Falah**, None; **J.-A. Sahel**, None; **F. Sennlaub**, None; **M. Benchaboune**, None; **M. Ullern**, None; **M. Paques**, None

References

1. Augood CA, Vingerling JR, de Jong PT, et al. Prevalence of age-related maculopathy in older Europeans: the European Eye Study (EUREYE). *Arch Ophthalmol*. 2006;124:529–535.
2. Klein R, Chou CF, Klein BE, Zhang X, Meuer SM, Saaddine JB. Prevalence of age-related macular degeneration in the US population. *Arch Ophthalmol*. 2011;129:75–80.
3. Haines JL, Hauser MA, Schmidt S, et al. Complement factor H variant increases the risk of age-related macular degeneration. *Science*. 2005;308:419–421.
4. Sarks SH. Ageing and degeneration in the macular region: a clinico-pathological study. *Br J Ophthalmol*. 1976;60:324–341.
5. Penfold PL, Killingsworth MC, Sarks SH. Senile macular degeneration. The involvement of giant cells in atrophy of the retinal pigment epithelium. *Invest Ophthalmol Vis Sci*. 1986;27:364–371.
6. Sarks JP, Sarks SH, Killingsworth MC. Evolution of geographic atrophy of the retinal pigment epithelium. *Eye (Lond)*. 1988;2:552–577.
7. Cherepanoff S, McMenamin P, Gillies MC, Kettle E, Sarks SH. Bruch's membrane and choroidal macrophages in early and advanced age-related macular degeneration. *Br J Ophthalmol*. 2010;94:918–925.
8. Curcio CA, Medeiros NE, Millican CL. The Alabama Age-Related Macular Degeneration Grading System for donor eyes. *Invest Ophthalmol Vis Sci*. 1998;39:1085–1096.
9. Liang J, Williams DR, Miller DT. Supernormal vision and high-resolution retinal imaging through adaptive optics. *J Opt Soc Am*. 1997;14:2884–2892.
10. Querques G, Massamba N, Guigui B, et al. In vivo evaluation of photoreceptor mosaic in early onset large colloid drusen using adaptive optics. *Acta Ophthalmol*. 2012;90:e327–328.
11. Godara P, Siebe C, Rha J, Michaelides M, Carroll J. Assessing the photoreceptor mosaic over drusen using adaptive optics and SD-OCT. *Ophthalmic Surg Lasers Imaging*. 2010;41:41:S104–108.
12. Boretsky A, Khan F, Burnett G, et al. In vivo imaging of photoreceptor disruption associated with age-related macular degeneration: A pilot study. *Lasers Surg Med*. 2012;44:603–610.
13. Viard C, Nakashima K, Lamory B, Paques M, Levecq X, Chateau N. Imaging microscopic structures in pathological retinas using a flood-illumination adaptive optics retinal camera. *Proc SPIE*. 2011;7885:488–509.
14. Goldsmith NT. Deep focus: a digital image processing technique to produce improved focal depth in light microscopy. *Image Anal Stereol*. 2000;19:163–167.
15. Morgan JI, Dubra A, Wolfe R, Merigan WH, Williams DR. In vivo autofluorescence imaging of the human and macaque retinal pigment epithelial cell mosaic. *Invest Ophthalmol Vis Sci*. 2009;50:1350–1359.
16. Roorda A, Zhang Y, Duncan JL. High-resolution in vivo imaging of the RPE mosaic in eyes with retinal disease. *Invest Ophthalmol Vis Sci*. 2007;48:2297–2303.
17. Sunness JS, Bressler NM, Tian Y, Alexander J, Applegate CA. Measuring geographic atrophy in advanced age-related macular degeneration. *Invest Ophthalmol Vis Sci*. 1999;40:1761–1769.
18. Choudhry N, Giani A, Miller JW. Fundus autofluorescence in geographic atrophy: a review. *Semin Ophthalmol*. 2010;25:206–213.
19. Schmitz-Valckenberg S, Fleckenstein M, Scholl HP, Holz FG. Fundus autofluorescence and progression of age-related macular degeneration. *Surv Ophthalmol*. 2009;54:96–117.
20. Göbel AP, Fleckenstein M, Schmitz-Valckenberg S, Brinkmann CK, Holz FG. Imaging geographic atrophy in age-related macular degeneration. *Ophthalmologica*. 2011;226:182–190.
21. Holz FG, Bindewald-Wittich A, Fleckenstein M, et al. Progression of geographic atrophy and impact of fundus autofluorescence patterns in age-related macular degeneration. *Am J Ophthalmol*. 2007;143:463–472.
22. Weinberger AW, Lappas A, Kirschkamp T, et al. Fundus near infrared fluorescence correlates with fundus near infrared reflectance. *Invest Ophthalmol Vis Sci*. 2006;47:3098–3108.
23. Keilhauer CN, Delori FC. Near-infrared autofluorescence imaging of the fundus: visualization of ocular melanin. *Invest Ophthalmol Vis Sci*. 2006;47:3556–3564.
24. Kellner U, Kellner S, Weinitz S. Fundus autofluorescence (488 nm) and near-infrared autofluorescence (787 nm) visualize different retinal pigment epithelium alterations in patients with age-related macular degeneration. *Retina*. 2010;30:6–15.
25. Schmitz-Valckenberg S, Lara D, Nizari S, et al. Localisation and significance of in vivo near-infrared autofluorescent signal in retinal imaging. *Br J Ophthalmol*. 2011;95:1134–1139.
26. Paques M, Simonutti M, Augustin S, Goupille O, El Mathari B, Sahel JA. In vivo observation of the locomotion of microglial cells in the retina. *Glia*. 2010;58:1663–1668.

Investigative Ophthalmology & Visual Science